

Journal of Materials Chemistry A

Accepted Manuscript



This is an *Accepted Manuscript*, which has been through the Royal Society of Chemistry peer review process and has been accepted for publication.

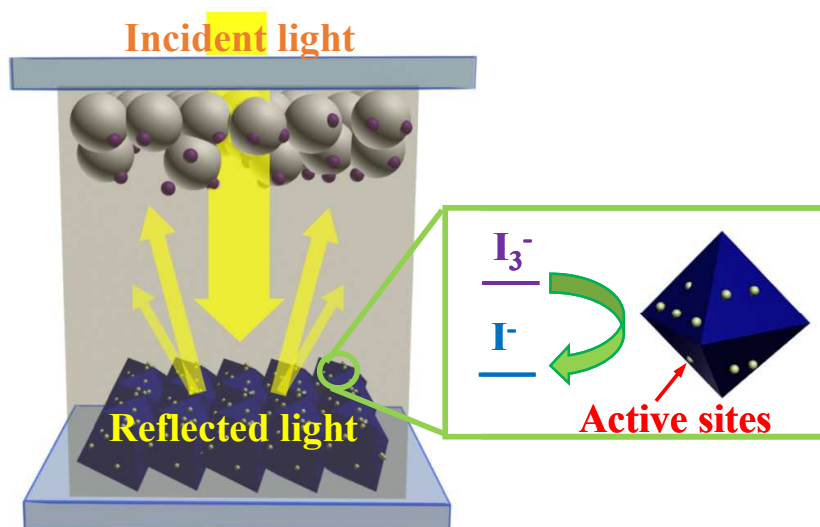
Accepted Manuscripts are published online shortly after acceptance, before technical editing, formatting and proof reading. Using this free service, authors can make their results available to the community, in citable form, before we publish the edited article. We will replace this *Accepted Manuscript* with the edited and formatted *Advance Article* as soon as it is available.

You can find more information about *Accepted Manuscripts* in the [Information for Authors](#).

Please note that technical editing may introduce minor changes to the text and/or graphics, which may alter content. The journal's standard [Terms & Conditions](#) and the [Ethical guidelines](#) still apply. In no event shall the Royal Society of Chemistry be held responsible for any errors or omissions in this *Accepted Manuscript* or any consequences arising from the use of any information it contains.

Platinum@Regular Indium Oxide Nanooctahedrons as Difunctional Counter Electrode for Dye-Sensitized Solar Cells

Bo Zhang*, Yu Hang Li, Ju Hua Zhong, Hai Min Zhang, Hui Jun Zhao and Hua Gui Yang*



Difunctional counter electrode composing of platinum nanoparticles supported on regular In_2O_3 nanooctahedrons demonstrates good catalytic activity and excellent light scattering.

Cite this: DOI: 10.1039/c0xx00000x

www.rsc.org/xxxxxx

ARTICLE TYPE

Platinum@Regular Indium Oxide Nanooctahedrons as Difunctional Counter Electrode for Dye-Sensitized Solar Cells†

Bo Zhang,^{*a,b} Yu Hang Li,^a Ju Hua Zhong,^b Xiao Hua Yang,^a Hai Min Zhang,^c Hui Jun Zhao^c and Hua Gui Yang^{*a,c}

Received (in XXX, XXX) Xth XXXXXXXXX 20XX, Accepted Xth XXXXXXXXX 20XX

DOI: 10.1039/b000000x

Platinum (Pt) nanoparticles below 2 nm loaded on In₂O₃ nanooctahedrons were prepared with the assistance of polymer ligands, and applied as an efficient difunctional counter electrode (CE) material for dye-sensitized solar cells (DSCs). Owing to the excellent light scattering performance of regular nanooctahedrons, the light harvesting efficiency was significantly increased, resulting in the noticeable 19.5% enhancement of energy conversion efficiency.

1. Introduction

Dye-sensitized solar cells (DSCs) have been regarded as a promising candidate for the next-generation photovoltaic devices due to their low cost, easy fabrication, and relatively high light-to-electric energy conversion efficiency.^{1, 2} In order to enhance the efficiency of DSCs, numerous advances have been made on developing sensitizing dyes,² electrolytes³⁻⁵, catalysts on counter electrodes (CEs)⁶⁻¹⁰ and new cell structures.¹¹⁻¹³ Moreover, correct optical design is essential to achieve high efficiency with solar cells, and the DSCs are no exception. One of the most common principles is trying to boost the light absorption by the various light-trapping or back-reflection techniques. These photon management techniques used in DSCs include difunctional photoanode with three-dimensional light scattering structure,¹⁴⁻¹⁶ plasmonic particles or structure in TiO₂ photoanode film,^{17, 18} back scattering layer or nanostructure at the TiO₂/electrolyte interface,^{19, 20} modified electrolytes²¹ and back scattering layer at CEs.^{22, 23} For example, Wang *et al.*¹⁹ introduced a scattering layer of cubic CeO₂ nanoparticles at the TiO₂ anode and achieved an efficient light harvesting efficiency. However, the study of CEs with light back-reflection and electrocatalytic activity for triiodide (I₃⁻) reduction difunction has rarely reported. Diao *et al.*²² applied mirror-like platinum (Pt) electrode as CE with specular reflection function. In this case, the CE has two functions - photo management and catalytic function, which means that the DSC device doesn't need extra light-scattering layer. However, the mirror-like Pt CE owns a high cost and specular reflection is not the best reflected pattern. According to the literature²⁴⁻²⁸, via bottom-up assembling of regular nanocrystals, tunable optical structures can be obtained. In this direction, one can prepare a Pt CE with light-scattering function via the assembling of Pt nanocrystals with well-defined facets, but it would consume much large amounts of Pt.

Herein, we for the first time proposed that we could explore Pt catalyst on regular support as efficient CE with light-scattering function, which takes the advantages of excellent physical

property of the support such as the high electric conductivity¹⁰ and regular structure for light-scattering. Also the Pt nanoparticles loaded on regular carrier with small size could increase the utilization efficiency and electrocatalytic activity of the Pt catalyst (see Fig. 1). Following this proposal, we prepared size-controlled Pt nanoparticles loaded on regular In₂O₃ (Pt@In₂O₃) nanooctahedrons using polymer as stabilizer. The application of the Pt@In₂O₃ in CEs resulted in about 18.7% enhancement of the short-circuit current density (J_{sc}) of DSCs. We attribute this improvement to the efficient light harvesting via the light scattering of regular In₂O₃ nanooctahedrons supporters.

2. Experimental

2.1 Materials

1-octadecene (90%), and oleic acid (90%) were purchased from Sigma-Aldrich. Chloroplatinic acid hexahydrate (analytical reagent grade) and Sodium borohydride (96%, analytical reagent grade) were obtained from Sinopharm Chemical Reagent Co. Ltd. Indium (III) acetate (99.99%) was purchased from Alfa.

2.2 Synthesis of In₂O₃ nanooctahedrons

In₂O₃ nanooctahedrons were prepared according to the literature²⁷. And the details are as follows: Under magnetic stirring and heating to 90 °C, 1.0 mmol indium (III) acetate was dissolved in mixed 1.0 mL oleic acid and 4.0 mL 1-octadecene to form 1.0 mmol indium oleate. The resulting colorless solution was then degassed under vacuum at 90 °C for 15 min followed by quickly heating to 320 °C. By maintaining at this temperature for 30 min, a milky white solution was obtained. The product was collected by centrifugation, washed with hexane and alcohol several times.

2.3 Synthesis of Pt@In₂O₃ samples

In a typical synthesis of Pt@In₂O₃ samples, 25 mg of In₂O₃ and 100 mg of poly(methacrylic acid) (PMAA) were added into a screw-neck glass bottle containing chloroplatinic acid solution (5 mL, 1 mg/mL), where PMAA were synthesized according to the

literature²⁹. After the suspension becoming uniform by sonication, 0.5 mL of freshly prepared sodium borohydride (NaBH₄) aqueous solution (10 mg/mL) was injected for reducing chloroplatinic acid under vigorously stirring, and another 0.5 mL of freshly prepared NaBH₄ solution was injected after 2~3 hours, kept stirring overnight. The Pt loading amount was explored by a Varian 710ES Inductively Coupled Plasma Atomic Emission Spectrometry (ICP-AES). This sample was named as 3.9wt%Pt@In₂O₃. In order to control the size of loaded Pt nanoparticles, the amount of ligand was increased from 100 mg to 200 mg, 400 mg and so on, keeping the same of other factors, and the obtained samples were named as 2.9wt%Pt@In₂O₃ and 0.7wt%Pt@In₂O₃, respectively. It has been approved that as the amount of ligand increased, the Pt loading decreased.

2.4 Preparation of dye-covered nanocrystalline-TiO₂ electrodes

To prepare the DSC working electrodes, the FTO glass was used as current collector (8 Ω/square, Nippon Sheet Glass, Japan). The commercially-available TiO₂ powders, P25 (Degussa, Germany), was used as raw material. A 12 μm thick layer of P25 was loaded on FTO by screen printer technique³⁰. After sintering at 500 °C for 30 min, the TiO₂-loaded FTO were immersed in a 5×10⁻⁴ M solution of N719 dye (Solaronix SA, Switzerland) in acetonitrile/*tert*-butyl alcohol (V/V=1/1) for 20-24 h to complete the sensitizer.

2.5 Preparation of counter electrodes

The 3.9wt%Pt@In₂O₃, 2.9wt%Pt@In₂O₃ and 0.7wt%Pt@In₂O₃ pastes were fabricated as follows: 100 mg Pt@In₂O₃ sample was mixed with 0.8 g anhydrous terpineol and 1.12 g ethyl celluloses in ethanol (10 wt%), followed by stirring and sonication. The contents in dispersion were concentrated by evaporator, and the solid content was reached to 9.8 wt%. A single layer of Pt@In₂O₃ paste was loaded on FTO by screen-printing procedure with a geometric area of about 0.36 cm² and heated under airflow at 450 °C for 30 min. The Pt-electrode was prepared by drop-casting 0.5 mM H₂PtCl₆/ethanol solution on the clean FTO conductive glass, and was then sintered in a muffle furnace at 450 °C for 30 min.

2.6 DSCs assembling

The counter electrode and dye-covered TiO₂ electrode were assembled into a sandwich type cell and sealed with a hot-melt gasket of 25 μm (Surlyn 1702, DuPont). A drop of the electrolyte, which is prepared via dissolving 0.60 M 1-butyl-3-methylimidazolium iodide, 0.03 M I₂, 0.50 M 4-*tert*-butyl pyridine, and 0.10 M guanidinium thiocyanate in acetonitrile, was put on the hole in the painted counter electrode. Then the electrolyte was introduced into the cell via vacuum backfilling. The dummy cells for electrochemical impedance spectra measurements were assembled with two identical Pt@In₂O₃ CEs or Pt loaded FTO, and the electrolyte was the same as the above.

2.7 Characterization

The morphology and structure of the samples were characterized by high-resolution transmission electron microscopy (HRTEM, JEOL 2100, 200 kV) and field emission scanning electron microscopy (FESEM, HITACHI S4800). The Pt loading amount

was explored by a Varian 710ES ICP-AES. The diffuse reflectance of the four CEs were scanned on a Cary 500 (Varian, USA) spectrophotometer equipped with an integrating sphere accessory. The IPCE spectra were measured with a Model SR830 DSP Lock-In Amplifier, a Model SR540 Optical Chopper (Stanford Research Corporation, USA), a 7IL/PX150 xenon lamp with power supply and a 7ISW301 Spectrometer. The photocurrent–voltage performance of the DSCs were measured with a Keithley digital source meter (Keithley 2400, USA) and simulated under AM 1.5 illumination. The power of the simulated light was calibrated to 100 mW·cm⁻² using a Newport Oriel PV reference cell system (model 91150 V). The electrochemical impedance spectra (EIS) experiments were measured with dummy cells in the dark by using an electrochemical workstation (Parstat 2273, Princeton). The frequency range of EIS experiments was from 100 mHz to 1 MHz with an AC modulation signal of 10 mV and bias DC voltage of 0.60 V. The obtained EIS curves were fitted by the ZSimpWin software. Cyclic voltammetry (CV) was conducted in a three-electrode system in an acetonitrile solution of 0.1 M LiClO₄, 10 mM LiI, and 1 mM I₂ at a scanning rate of 20 mV s⁻¹. The working electrodes were Pt@In₂O₃ and Pt loaded FTO. The Ag/Ag⁺ couple was employed as reference electrode, and the counter electrode was a platinum foil.

3. Results and discussion

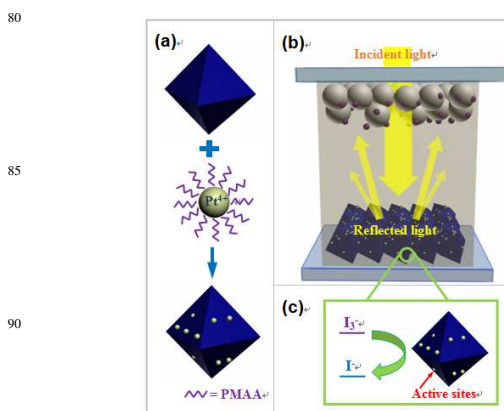


Fig. 1 Schematic of the proposed difunctional CE: (a) synthesis of Pt@In₂O₃ nano-octahedrons with the assistance of poly(methacrylic acid) (PMAA); (b) DSCs assembled with difunctional CE having light-scattering functionality; (c) Pt nanoparticles loaded on In₂O₃ nano-octahedrons serving as active sites for I₃⁻ reduction.

Since the high electric conductivity of supporter is indispensable to supported electrocatalyst, we choose In₂O₃ as supporter. Regular In₂O₃ nano-octahedrons were synthesized according to the literature²⁷, and the morphology of In₂O₃ nano-octahedrons sample was detected by SEM. Further, size-controlled Pt nanoparticles were loaded on In₂O₃ nano-octahedrons with the assistance of PMAA. The light scattering effect was evaluated by measuring the Pt@In₂O₃ films deposited on FTO conductive glass via screen-printing procedure comparing with the typical Pt film deposited on FTO via thermal decomposition. The films on FTO were scanned on a Cary 500 spectrophotometer equipped with an integrating sphere accessory, and the results are shown in Fig. 2. It can be seen that in comparison with the typical Pt film,

the Pt@In₂O₃ samples show remarkable improvement of light reflectance in the light range from 300 to 800 nm, especially from 300 to 600 nm. In particular, the reflectance of 0.7wt%Pt@In₂O₃ has increased 230% at the wavelength around 400 nm compared to Pt film. The digital images in Fig. S1 show that Pt CE is black and 0.7wt%Pt@In₂O₃ is white with effective light scattering, which benefits the light harvesting of DSCs. This remarkable reflectance is obviously attributed to the strong light scattering with the regular octahedrons.

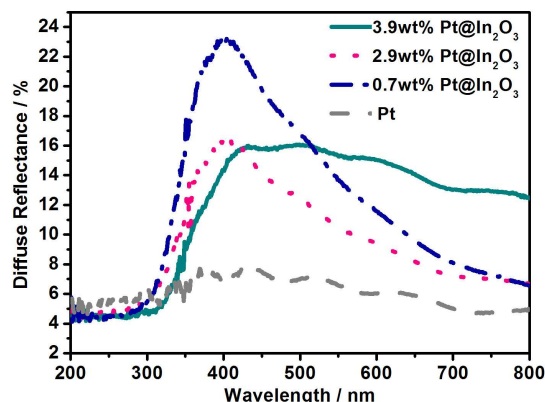


Fig. 2 UV-vis diffuse reflectance of Pt@In₂O₃ electrodes and the commonly used Pt electrode.

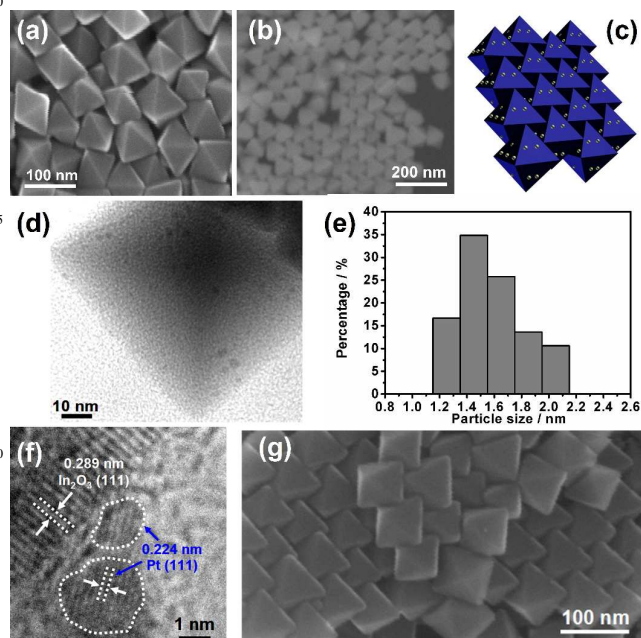


Fig. 3 (a) SEM image of In₂O₃ nanooctahedrons; (b,c) SEM image and the corresponding diagram of self-assembly of 0.7wt%Pt@In₂O₃ sample; (d, f) TEM and HRTEM images of 0.7wt%Pt@In₂O₃ sample; (e) Histogram showing the size distribution of Pt nanoparticles based on a count of 120 Pt nanoparticles in five different sampling areas; (g) surface SEM micrograph of 0.7wt%Pt@In₂O₃ sample screening-printed on FTO with self-assembled structure.

The as-prepared In₂O₃ nanocrystals and Pt loaded In₂O₃ nanocrystals were first characterized by SEM. As shown in the SEM images in Fig. 3a, In₂O₃ nanocrystals have a uniform regular octahedral morphology. While, after Pt nanoparticles were loaded, Fig. 3b shows that not only the uniform regular octahedral morphology of In₂O₃ has not been changed, but also the regular self-assembled structure of 0.7wt%Pt@In₂O₃ sample means that the loaded Pt nanoparticles should not have influence on light-scattering effect of the support, and the corresponding self-assembled model is shown in Fig. 3c. The loaded Pt nanoparticles and dispersion of 0.7wt%Pt@In₂O₃ sample were characterized via TEM and HRTEM, and the results are shown in Fig. 3d-f (results of other samples are shown in Fig. S2 in SI). Fig. S2 presents that as the amount of ligand was increased, the particle size of loaded Pt nanoparticles decreased, which is consistent with the literature.³¹ As shown in Fig. 3e, 0.7wt%Pt@In₂O₃ exhibits a narrow particle size distribution and the particle owns an average diameter of 1-2 nm. From Fig. 3f, HRTEM result shows that the particles on In₂O₃ are crystalline and the lattice spacing of the fringe correspond to the (100) plane of Pt, confirming the loaded composition. The as-prepared Pt@In₂O₃ samples were mixed with ethanol, ethyl cellulose and terpineol to make a paste using a rotary evaporator. Then, the Pt@In₂O₃ films were screen-printed on the FTO glass with the obtained paste, and then sintered at 450 °C. The surface structures of 0.7wt%Pt@In₂O₃ on FTO were characterized using SEM and the images were given in Fig. 3g. Part of the surface in Fig. 3g showed a self-assembled structure same as that shown in Fig. 3b-c, which benefits the light-scattering effect of the CEs.

The supported catalysts as CEs were subsequently assembled into DSCs to investigate the scattering effect on photovoltaic performance in comparison to the common used Pt CE from thermal decomposition. Fig. 4a displays the photocurrent-voltage (*J-V*) curves for DSCs with pure Pt, 3.9wt%Pt@In₂O₃, 2.9wt%Pt@In₂O₃, 0.7wt%Pt@In₂O₃ and pure In₂O₃ nanooctahedrons as CEs, and the detailed photovoltaic parameters are summarized in Table 1. As shown in Table 1, *J*_{sc} of the DSCs assembled with the three Pt@In₂O₃ samples as CEs are significantly enhanced. Especially, the energy conversion efficiency (η) and *J*_{sc} of DSCs with 0.7wt%Pt@In₂O₃ CE reach to 8.10% and 17.50 mA cm⁻², which are respectively approximately 19.5% and 18.7% greater than those of the DSCs with typical Pt CEs (6.78%, 14.75 mA cm⁻²). We have also prepared several samples with different Pt loading amount between 3.9wt% and 0, and optimal loading amount is 0.7wt%. The incident-photon-to-current conversion efficiency (IPCE) spectra offer detailed information on the light harvesting of DSCs and the light scattering efficiency can be explained by the IPCE value in the longer wavelength region.^{19, 32} The IPCE results in Fig. 4b show that the overall IPCE increases considerably by using Pt@In₂O₃ CEs, especially the 0.7wt%Pt@In₂O₃, which is in good agreement with the difference of *J*_{sc} values. These interesting results demonstrate that the DSCs with Pt@In₂O₃ CEs possess more effective light harvesting, which should be attributed to the effective light scattering of regular nanooctahedrons. Also, it can be obtained that the fill factors (*FF*) of the DSCs with 3.9wt%Pt@In₂O₃ and 2.9wt%Pt@In₂O₃ are lower than that of the typical DSCs with Pt CE. According to the literature,³³ the

increased electron transfer rate from the TiO_2 to the I_3^- is the obvious possible cause for a low FF . Whereas, the formed densified structure of CEs by the packing In_2O_3 nanooctahedrons could lead to the increased difficulty of electrolyte infiltration into the pores,³⁴ which would inhibit the I_3^- reduction. This may be the reason for the low FF of DSCs with $\text{Pt@In}_2\text{O}_3$ CEs. But, as the particle size of supported Pt nanoparticles decreases, the electrocatalytic activity of $\text{Pt@In}_2\text{O}_3$ samples may be increased. When the Pt particle size is about 1-2 nm, the FF of DSCs with 0.7wt%Pt@ In_2O_3 CE reaches to 0.62, similar to that of typical Pt CE (0.61). In this situation, the I_3^- species could be reduced in time, making up the weakness of electrolyte infiltration, so the low concentration of I_3^- ions would inhibit the electron transfer from the TiO_2 to the I_3^- , resulting in the high FF .

In order to elucidate the electrocatalytic activities of different CE materials for I_3^- reduction, EIS and CV measurements of

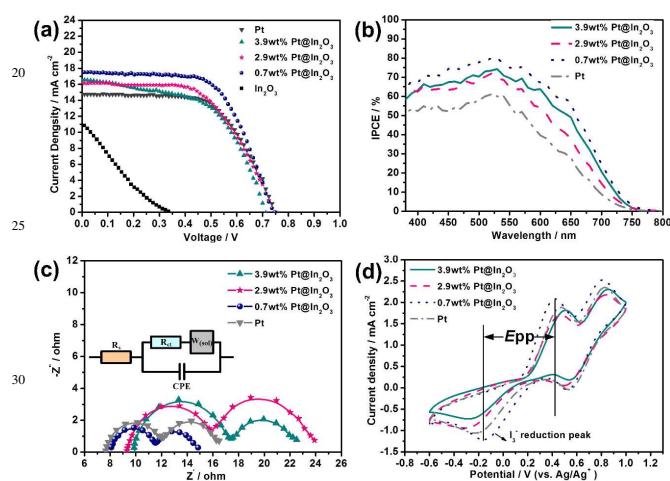


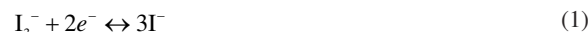
Fig. 4 (a) Photocurrent-voltage (J - V) curves of DSCs fabricated with pure In_2O_3 , three $\text{Pt@In}_2\text{O}_3$ and Pt as CEs; (b) IPCE spectra of the corresponding DSCs showing in (a); (c) electrochemical impedance spectra of the symmetrical cells fabricated with two identical CEs, and the insert gives the equivalent circuit; (d) cyclic voltammograms of 3.9wt%Pt@ In_2O_3 , 2.9wt%Pt@ In_2O_3 , 0.7wt%Pt@ In_2O_3 , and pure Pt deposited on FTO.

Table 1 Photovoltaic parameters of DSCs with different counter electrodes and the simulated data from EIS spectra.

Samples	J_{sc} / mA cm ⁻²	V_{oc} / V	FF	η / %	R_s / Ω	R_{ct} / Ω
In_2O_3	11.13	336	0.26	0.96	9.52	379.4
0.7wt%Pt@ In_2O_3	17.50	749	0.62	8.10	8.16	3.23
2.9wt%Pt@ In_2O_3	16.19	748	0.58	6.90	9.47	6.28
3.9wt%Pt@ In_2O_3	16.59	712	0.56	6.57	10.01	7.16
Pt	14.75	748	0.61	6.78	7.81	3.88

$\text{Pt@In}_2\text{O}_3$ and Pt CEs were carried out, and the results are shown in Fig. 4c and Fig. 4d, and the EIS of pure In_2O_3 nanooctahedrons is given in Fig. S3 in SI. The EIS parameters were determined by

fitting the impedance spectra using the ZSimpWin software via the circuit model inserted in Fig. 4c, and were summarized in Table 1. The high-frequency intercept on the real axis represents the series resistance (R_s), which is mainly composed of the bulk resistance of CEs materials, resistance of FTO glass substrate, and contact resistance, *etc.* It can be seen that R_s of three $\text{Pt@In}_2\text{O}_3$ samples are larger than that Pt CE, which should be damage to the J_{sc} . This result confirms that the enhanced J_{sc} of DSCs with $\text{Pt@In}_2\text{O}_3$ CEs should be attributed to the effective light scattering of regular nanooctahedrons. R_{ct} is a measure of the ease of electron exchange between the electrode and the electrolyte and thus varies inversely with the I_3^- reduction activity of the CEs³⁵. From Table 1, R_{ct} of 0.7wt%Pt@ In_2O_3 is 3.23 Ω , which is smaller than that of Pt (3.88 Ω), 3.9wt%Pt@ In_2O_3 (6.28 Ω) and 2.9wt%Pt@ In_2O_3 (7.16 Ω), which means that 0.7wt%Pt@ In_2O_3 has a higher electrocatalytic activity for I_3^- reduction than other samples, which is benefit to the increase of FF and η . While the high R_{ct} of pure In_2O_3 nanooctahedrons (379.4 Ω) indicates that it has nearly no catalytic activity for I_3^- reduction, and hence the η of DSCs with it is very low. It can be obtained that the high loading amount of Pt does not help to enhance the electrocatalytic activity. Instead, 0.7wt%Pt@ In_2O_3 with the smallest Pt particle size and least loading amount has the best electrocatalytic activity, which means that the smaller the size of catalyst, the higher the electrocatalytic activity, and the more the utilization degree of it which may be due to its geometric effect.³⁶ From the CV result in Fig. 4d, it can be seen that both the $\text{Pt@In}_2\text{O}_3$ and Pt electrode have similar CV curves with two pair redox peaks. The relatively negative pair corresponds to redox reaction (1), whereas the more positive pair is assigned to the redox reaction (2).



The electrocatalytic activity of the CEs is related to the negative pair. A higher reduction peak current density corresponding to I_3^- reduction and a lower peak-to-peak voltage separation (E_{pp}) indicate a higher electrocatalytic activity.^{10, 37, 38} The relatively high cathodic peak and large E_{pp} observed for 0.7wt%Pt@ In_2O_3 with respect to Pt and other electrodes suggest a higher electrocatalytic activity for I_3^- reduction than Pt and other samples, which is in consistent with the results of photovoltaic performance and EIS. The optimized Pt nanoparticles with small size supported on In_2O_3 not only decreased the consumption of Pt, but also enhanced the electrocatalytic activity. Combined with the excellent light scattering of In_2O_3 nanooctahedrons, the difunctional $\text{Pt@In}_2\text{O}_3$ CEs facilitate the high photovoltaic performance of the DSCs with it.

Conclusions

In summary, for the first time, we have demonstrated that Pt loaded on In_2O_3 nanooctahedrons as difunctional CEs with light scattering effect can significantly improve the J_{sc} and energy conversion efficiency of DSCs. The supported catalyst not only improves the utilization of Pt and reduces the cost, but also makes full use of the regular morphology of the support for light scattering. Compared with the reference DSCs using typical Pt

CEs, the DSCs assembled with 0.7wt%Pt@In₂O₃ CEs exhibited a remarkable 19.5% improvement in energy conversion efficiency. More importantly, this finding provides a new approach for efficiency improvement of DSCs via designing difunctional CEs with light scattering effect.

Acknowledgement

This work was financially supported by National Natural Science Foundation of China (21373083, 21203061), SRF for ROCS, SEM, SRFDP, Programme for Professor of Special Appointment (Eastern Scholar) at Shanghai Institutions of Higher Learning, Fundamental Research Funds for the Central Universities (WD1313009, WM1314018, WD1214036), and China Postdoctoral Science Foundation (2012M511056, 2013T60425).

Notes and references

¹⁵ ^a Key Laboratory for Ultrafine Materials of Ministry of Education, School of Materials Science and Engineering, East China University of Science and Technology, 130 Meilong Road, Shanghai, 200237 (China). Fax: (+86)21-6425-2127; Tel: (+86)21-6425-2127; E-mail: hgyang@ecust.edu.cn

²⁰ ^b Department of Physics, East China University of Science and Technology, 130 Meilong Road, Shanghai, 200237 (China). Fax: (+86)21-6425-1493; Tel: (+86)21-6425-1493; E-mail: bo.zhang@ecust.edu.cn

²⁵ † Supporting Information available: Digital images of counter electrodes; TEM of Pt@In₂O₃ samples; EIS of DSC with In₂O₃ as CE.

1. B. O'Regan and M. Grätzel, *Nature*, 1991, **353**, 737-740.
2. A. Yella, H.-W. Lee, H. N. Tsao, C. Yi, A. K. Chandiran, M. K. Nazeeruddin, E. W.-G. Diau, C.-Y. Yeh, S. M. Zakeeruddin and M. Grätzel, *Science*, 2011, **334**, 629-634.
3. J.-H. Yum, E. Baranoff, F. Kessler, T. Moehl, S. Ahmad, T. Bessho, A. Marchioro, E. Ghadiri, J.-E. Moser, C. Yi, M. K. Nazeeruddin and M. Grätzel, *Nature Communications*, 2012, **3**, 631.
4. T. Daeneke, Y. Uemura, N. W. Duffy, A. J. Mozer, N. Koumura, U. Bach and L. Spiccia, *Adv. Mater.*, 2012, **24**, 1222-1225.
5. T. Daeneke, T.-H. Kwon, A. B. Holmes, N. W. Duffy, U. Bach and L. Spiccia, *Nature Chemistry*, 2011, **3**, 211-215.
6. Y. Hou, D. Wang, X. Yang, W. Fang, B. Zhang, H. Wang, P. Hu, H. Zhao and H. Yang, *Nature Communications*, 2013, **4**, 1583.
7. B. Zhang, D. Wang, Y. Hou, S. Yang, X. Yang, J. Zhong, J. Liu, H. Wang, P. Hu, H. Zhao and H. Yang, *Scientific Reports*, 2013, **3**, 1836.
8. X. Chen, Y. Hou, B. Zhang, X. H. Yang and H. G. Yang, *Chem. Commun.*, 2013, **49**, 5793-5795.
9. L. Cheng, Y. Hou, B. Zhang, S. Yang, J. W. Guo, L. Wu and H. G. Yang, *Chem. Commun.*, 2013, **49**, 5945-5947.
10. J. W. Guo, B. Zhang, Y. Hou, S. Yang, X. H. Yang and H. G. Yang, *Journal of Materials Chemistry A*, 2013, **1**, 1982-1986.
11. J. H. Heo, S. H. Im, J. H. Noh, T. N. Mandal, C.-S. Lim, J. A. Chang, Y. H. Lee, H.-j. Kim, A. Sarkar, K. NazeeruddinMd, M. Gratzel and S. I. Seok, *Nat. Photonics* 2013, **7**, 486-491.
12. M. M. Lee, J. Teuscher, T. Miyasaka, T. N. Murakami and H. J. Snaith, *Science*, 2012, **338**, 643-647.

13. I. Chung, B. Lee, J. He, R. P. H. Chang and M. G. Kanatzidis, *Nature*, 2012, **485**, 486-489.
14. N. Tétreault, É. Arseneault, L.-P. Heiniger, N. Soheilnia, J. Brillet, T. Moehl, S. Zakeeruddin, G. A. Ozin and M. Grätzel, *Nano Lett.*, 2011, **11**, 4579-4584.
15. J. Shi, Y. Hara, C. Sun, M. A. Anderson and X. Wang, *Nano Lett.*, 2011, **11**, 3413-3419.
16. S. G. Foster and S. John, *Energy Environ. Sci.*, 2013.
17. I. K. Ding, J. Zhu, W. Cai, S.-J. Moon, N. Cai, P. Wang, S. M. Zakeeruddin, M. Grätzel, M. L. Brongersma, Y. Cui and M. D. McGehee, *Advanced Energy Materials*, 2011, **1**, 52-57.
18. J. Xi, Q. Zhang, K. Park, Y. Sun and G. Cao, *Electrochim. Acta* 2011, **56**, 1960-1966.
19. L. Wang, *Chem. Commun.*, 2012, **48**, 7386-7388.
20. J. Kim, J. K. Koh, B. Kim, J. H. Kim and E. Kim, *Angew. Chem. Int. Ed.*, 2012, **51**, 6864-6869.
21. M. Wang, X. Pan, X. Fang, L. Guo, W. Liu, C. Zhang, Y. Huang, L. Hu and S. Dai, *Adv. Mater.*, 2010, **22**, 5526-5530.
22. L.-L. Li, C.-W. Chang, H.-H. Wu, J.-W. Shiu, P.-T. Wu and E. Wei-Guang Diau, *J. Mater. Chem.*, 2012, **22**, 6267-6273.
23. B. Lee, D.-K. Hwang, P. Guo, S.-T. Ho, D. B. Buchholtz, C.-Y. Wang and R. P. H. Chang, *J. Phys. Chem. B*, 2010, **114**, 14582-14591.
24. J. Henzie, M. Grünwald, A. Widmer-Cooper, P. L. Geissler and P. Yang, *Nat. Mater.*, 2012, **11**, 131-137.
25. S. Gwo, M.-H. Lin, C.-L. He, H.-Y. Chen and T. Teranishi, *Langmuir*, 2012, **28**, 8902-8908.
26. X.-Y. Zhang, A. Hu, T. Zhang, W. Lei, X.-J. Xue, Y. Zhou and W. W. Duley, *ACS Nano*, 2011, **5**, 9082-9092.
27. E. Ye, S.-Y. Zhang, S. Hon Lim, S. Liu and M.-Y. Han, *PCCP* 2010, **12**, 11923-11929.
28. W. Lu, Q. Liu, Z. Sun, J. He, C. Ezeolu and J. Fang, *J. Am. Chem. Soc.*, 2008, **130**, 6983-6991.
29. Z. Li, B. Tan, M. Allix, A. I. Cooper and M. J. Rosseinsky, *Small*, 2008, **4**, 231-239.
30. S. Ito, P. Chen, P. Comte, M. K. Nazeeruddin, P. Liska, P. Péchy and M. Grätzel, *Prog. Photovoltaics Res. Appl.*, 2007, **15**, 603-612.
31. I. Hussain, S. Graham, Z. Wang, B. Tan, D. C. Sherrington, S. P. Rannard, A. I. Cooper and M. Brust, *J. Am. Chem. Soc.*, 2005, **127**, 16398-16399.
32. F. Huang, D. Chen, X. L. Zhang, R. A. Caruso and Y.-B. Cheng, *Adv. Funct. Mater.*, 2010, **20**, 1301-1305.
33. D. Cahen, G. Hodes, M. Grätzel, J. F. Guillemoles and I. Riess, *J. Phys. Chem. B*, 2000, **104**, 2053-2059.
34. S. Nakade, T. Kanzaki, Y. Wada and S. Yanagida, *Langmuir*, 2005, **21**, 10803-10807.
35. M. Wang, A. M. Anghel, B. Marsan, N.-L. Cevey Ha, N. Pootrakulchote, S. M. Zakeeruddin and M. Grätzel, *J. Am. Chem. Soc.*, 2009, **131**, 15976-15977.
36. MurdochM, G. I. N. Waterhouse, M. A. Nadeem, J. B. Metson, M. A. Keane, R. F. Howe, LlorcaJ and IdrissH, *Nature Chemistry*, 2011, **3**, 489-492.
37. Z. Yang, M. Liu, C. Zhang, W. W. Tjiu, T. Liu and H. Peng, *Angew. Chem. Int. Ed.*, 2013, **52**, 3996-3999.
38. F. Gong, H. Wang, X. Xu, G. Zhou and Z.-S. Wang, *J. Am. Chem. Soc.*, 2012, **134**, 10953-10958.

